Modeling of Hyperconcentrated Sediment-Laden Floods in Lower Yellow River

J. R. Ni[1]; H. W. Zhang[2]; A. Xue[3]; S. Wieprecht[4]; and A. G. L. Borthwick[5]

Abstract: This paper presents a rapid forecast model for simulating hyperconcentrated sediment-laden floods in the Lower Yellow River. The model is a hybrid of a conventional one-dimensional mathematical model for unsteady sediment-laden flow and an artificial neural networks model for encapsulation of numerical results. The former provides detailed river flood routing information under typical scenarios, whereas the latter extracts modeling outputs from the former and establishes a station-specific model for efficient flood forecasting. Three typical floods that occurred in the Lower Yellow River in 1977, 1982, and 1996 are simulated. Not only the hybrid model predictions are found to be in close agreement with measured data, but also the computational speed is significantly enhanced. It is found that sediment transport is of significance with regard to the flooding behavior of hyperconcentrated flows. Therefore, the model presented herein is of particular use for rivers with high sediment concentration.

DOI: 10.1061/(ASCE)0733-9429(2004)130:10(1025)

CE Database subject headings: Mathematical Models; Neural networks; Flood routing; China; Rivers; Sedimentation.

Introduction

The Yellow River, the second largest river in China (Fig. 1), is noted for its high sediment concentration; in fact, the maximum recorded sediment concentration in the Yellow River to date has been 1,650 kg/m^3 (Chien 1988). In cases where the Yellow River has a sediment concentration above 100 kg/m^3, Chen et al. (2000) categorize the flood as a hyperconcentrated sediment-laden flood (HCSLF). This type of flood is quite different from a low-concentrated sediment-laden flood (LCSLF) with regard to flow characteristics, flood routing, and consequential effects on sediment transport and river bed deformation.

In the Lower Yellow River, the consequences of a HCSLF on sediment transport and river deformation, such as channel erosion and deposition, are quite different to that of LCSLF. Fig. 2 presents the spatially averaged mean deposition rate of sediment against the spatially averaged mean sediment concentration obtained by analyzing field data from stations located between Tiexie and Gaocun. A polynomial fit to the rather limited data is also given in Fig. 2 indicating that the deposition rate is fairly low at about 0.3×10^{11} kg for sediment concentrations below about 60 kg/m^3. At higher sediment concentrations the deposition rate appears to increase nonlinearly. It is quite obvious that the amount of deposition increases more rapidly during HCSLF than LCSLF events. From Tiexie to Gaocun there are many measurement stations, and it is well established that the river cross-section changes form often during a HCSLF. This is typical behavior of a braided river dominated by flood events, and implies that there may be a potential increase of flood risk in the whole Lower Yellow River. Under these circumstances, it is necessary to be able to predict consequences very quickly at any specific station. Therefore, rapid forecasting of sediment concentration, discharge, and water level, which are closely related to the consequences of floods, is vital.

Many difficulties arise in the prediction, prevention, and control of hyperconcentrated floods due to the uncertainties encountered in modeling turbulent free surface flows with high sediment concentration. For example, there are no explicit rating curves expressing the relationship between water level and flow discharge in the Lower Yellow River due to changes in sediment concentration during floods (Fig. 3).

To date, many mathematical models (e.g., Cunge et al. 1980; Lin et al. 1983; Lin and Falconer 1996) have been developed for low-concentrated sediment-laden flows, but few are applicable to hyperconcentrated floods. To describe the complex stage discharge behavior, such as shown in Fig. 3, new approaches are needed to take into account sediment effects in hyperconcentrated floods. Wei (1990) developed a two-dimensional mathematical model for sediment-laden flow in the Lower Yellow River. Zhang et al. (2001) analyzed characteristics of hyperconcentrated floods in the Lower Yellow River and proposed a one-dimensional sediment-laden flow model.

Conventional hydrodynamic and sediment transport models are satisfactory for reproducing typical (LCSLF) scenarios, but they are not very efficient for real time prediction of HCSLF. In recent years, the artificial neural networks (ANN) model approach has found wide applications in engineering science. Minns and

[1]Professor, Dept. of Environmental Engineering, Peking Univ., The Key Laboratory of Water and Sediment Sciences, MOE, Beijing 100871, China.

[2]Professor, Dept. of Hydraulic Engineering, Tsinghua Univ., Beijing 100084, China.

[3]Associate Professor, Dept. of Environmental Engineering, Peking Univ., The Key Laboratory of Water and Sediment Sciences, MOE, Beijing 100871, China.

[4]Senior Researcher, Dept. of River Morphology, Federal Institute of Hydrology, 56002 Koblenz, Germany.

[5]Professor, Dept. of Engineering Science, Oxford Univ., Parks Road, Oxford OXI 3PJ, U.K.

Note. Discussion open until March 1, 2005. Separate discussions must be submitted for individual papers. To extend the closing date by one month, a written request must be filed with the ASCE Managing Editor. The manuscript for this paper was submitted for review and possible publication on January 17, 2003; approved on March 15, 2004. This paper is part of the ***Journal of Hydraulic Engineering***, Vol. 130, No. 10, October 1, 2004. ©ASCE, ISSN 0733-9429/2004/10-1025–1032/$18.00.

Fig. 1. Lower Yellow River downstream of Sanmenxia

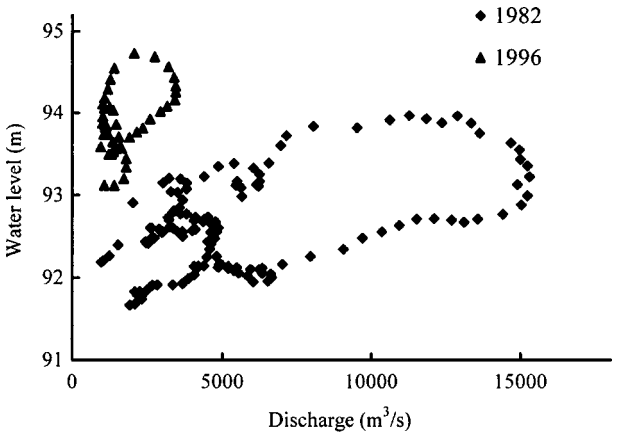

Fig. 3. Typical rating curves at Huayuankou

Hall (1996) used an ANN model to study the dynamic variation of precipitation and runoff processes in catchments. Hsu et al. (1995) compared results obtained from ANN to conventional mathematical models, and indicated that ANN is more efficient for the prediction of runoff characteristics. Li and Li (1999) established an ANN model for sediment-laden flows in rivers. Yonas and Michael (1999) investigated several types of ANN-agent architectures and proved their ability in encapsulating site-specific knowledge and data. Ni and Xue (2003) applied integrated ANN and hydrodynamic models associated with the geographical information system to control flood diversion in the Jingjiang diversion area.

The aforementioned studies demonstrate the apparent advantages of ANN in rapid prediction, feedback, and process control through encapsulation of knowledge from numerical models in large computational domains. In the present paper, an ANN is used to extract information from conventional hydrodynamic and sediment models, and the resulting hybrid model used to enhance the simulation of hyperconcentrated floods in the Lower Yellow River. The hybrid model provides detailed hydraulic information at any section under consideration and facilitates rapid response to varying flow and sediment conditions.

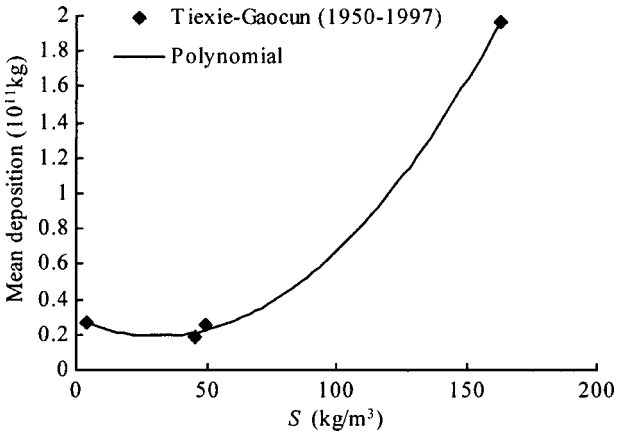

Fig. 2. Curve of sediment concentration and deposition from Tiexie to Gaocun

Numerical Modeling

Basic Equations and Parameters

The basic equations of one-dimensional unsteady sediment-laden flow are as follows:

$$\frac{\partial A_i}{\partial t} + \frac{\partial Q_i}{\partial x} - q_{Li} = 0 \tag{1}$$

$$\frac{\partial Q_i}{\partial t} + \frac{\partial}{\partial x}\left(\alpha_{1i}\frac{Q_i^2}{A_i}\right) + \alpha_{2i}\frac{Q_i}{A_i}q_{Li} + gA_i\left(\frac{\partial Z_i}{\partial x} + \frac{Q_i^2}{K_i^2}\right) = 0 \tag{2}$$

$$\frac{\partial}{\partial t}(A_iS_i) + \frac{\partial(A_iV_iS_i)}{\partial x} + \sum_{j=1}^{m}(K_{1ij}\alpha_{*ij}f_{1ij}b_{ij}S_{ij}\omega_{ij}) - \sum_{j=1}^{m}(K_{1ij}\alpha_{*ij}b_{ij}S_{*ij}\omega_{ij}) - S_{Li}q_{Li} = 0 \tag{3}$$

$$\frac{\partial Z_{bij}}{\partial t} - \frac{K_{1ij}\alpha_{*ij}}{\gamma_0}\omega_{ij}(f_{1ij}S_{ij} - S_{*ij}) = 0 \tag{4}$$

Eqs. (1) and (2) are continuity and momentum equations for fluid flow, respectively, and Eqs. (3) and (4) are the continuity equation for sediment transport and riverbed deformation, respectively. In Eq. (3) the first two terms relate to advection of suspended sediment, the third and fourth terms relate to sediment fluxes, and the fifth (source) term corresponds to the source-tye lateral sediment inflows to the system. In these equations, $i=1,2,\cdots N$ and N is the total number of cross sections along the river. $\Phi_i(\Phi=Q,A,q_L,\cdots)$ denotes the quantity at the ith cross section; each cross section is divided into several subsections, and $\Phi_{ij}(\Phi=K_1,\alpha_*,f_1,\cdots)$ stands for the quantity at the jth subsection of the ith cross section. Q=water discharge; A=cross sectional area; t=time; x=coordinate in flow direction; q_L=lateral water inflow per unit length; Z=water stage; g=gravitational acceleration; α_1 and α_2=momentum correction factor; K=discharge factor related to riverbed roughness; b=width; S=suspended sediment concentration by volume; S_L=lateral sediment inflow per unit length; V=velocity of water flow; Z_b=bed elevation; α_*=saturation recovery coefficient; ω=settling velocity of sediment particles; γ_0 is defined as weight of sediment; S_*=sediment carrying capacity; K_1=comprehensive coefficient; and f_1=subsaturation coefficient. The saturation recovery coefficient α_* denotes the ratio between

the bottom and average concentrations under equilibrium conditions, which is not a constant in this model and is evaluated using the following empirical expression obtained by integrating the sediment concentration over water depth (Zhang and Zhang 1992)

$$\alpha_* = \frac{1}{N_0}\exp\left(8.21\frac{\omega}{\kappa u_*}\right) \tag{5}$$

in which

$$N_0 = \int_0^1 f\left(\frac{\sqrt{g}}{c_n C},\eta\right)\exp\left(5.33\frac{\omega}{\kappa u_*}\text{arctg}\sqrt{\frac{1}{\eta}-1}\right)d\eta \tag{6}$$

and

$$f\left(\frac{\sqrt{g}}{c_n C},\eta\right) = 1 - \frac{3\pi\sqrt{g}}{8c_n C} + \frac{\sqrt{g}}{c_n C}(\sqrt{\eta-\eta^2} + \arcsin\sqrt{\eta}) \tag{7}$$

Herein κ, C and u_*=Karman constant, Chezy resistance coefficient, and friction velocity, respectively; η=relative depth; c_n =vortex coefficient (c_n=0.375κ); the Karman universal constant $\kappa = 0.4 - 1.68(0.365 - S_V)\sqrt{S_V}$, and, K_1=comprehensive coefficient. Based on similarity theory and movable bed models, K_1 is derived as follows (Zhang and Zhang 1992):

$$K_1 = \frac{1}{2.65}\kappa^{4.5}\left(\frac{u_*^{1.5}}{V^{0.5}\omega}\right)^{1.14} \tag{8}$$

The subsaturation coefficient f_1 is deduced from numerous experimental data and can be estimated from (Zhang et al. 2001)

$$f_1 = \left(\frac{S}{S_*}\right)^{[0.1/\text{arctg}(S/S_*)]} \tag{9}$$

To ensure that the model is capable of simulating both normal sediment-laden flows and hyperconcentrated flows in the Lower Yellow River, the following equation for the sediment carrying capacity is introduced (Zhang et al. 2001):

$$S_* = 2.5\left[\frac{(0.0022 + S_V)V^3}{\kappa\frac{\gamma_s - \gamma_m}{\gamma_m}gh\omega}\ln\left(\frac{h}{6D_{50}}\right)\right]^{0.62} \tag{10}$$

where S_V=particle volume fraction; h=water depth; D_{50} =median diameter of bed materials; γ_s=specific weight of sediment; and γ_m=specific weight of muddy water. The sediment settling velocity ω and Manning's roughness coefficient n are two important parameters in the modeling process. Allowing for the special conditions that pertain to the Lower Yellow River, the sediment settling velocity can be expressed as (Zhang et al. 2001)

$$\omega = \omega_0(1 - 1.25S_v)\left[1 + \frac{S_v}{2.25\sqrt{d_{50}}}\right]^{3.5} \tag{11}$$

and the Manning's coefficient can be estimated from (Zhang et al. 2001)

$$n = \frac{h^{1/6}}{\sqrt{g}}\left[\frac{c_n\frac{\delta_*}{h}}{0.49\left(\frac{\delta_*}{h}\right)0.77 + \frac{3\pi}{8}\left(1 - \frac{\delta_*}{h}\right)\left[\sin\left(\frac{\delta_*}{h}\right)^{0.2}\right]^5}\right] \tag{12}$$

in which δ_*=friction thickness, defined as

$$\delta_* = D_{50}\{1 + 10^{[8.1-13Fr^{0.5}(1-\text{Fr}^3)]}\} \tag{13}$$

The suspended sediment concentration profile and the distribution of the sediment particle's median diameter in the transverse direction are evaluated by the following expressions (Zhang et al. 2001):

$$\frac{S_{ij}}{S_i} = C_1\left(\frac{h_{ij}}{h_i}\right)^{[0.1-1.6(\omega/\kappa u_*)+1.3S_{Vi}]}\left(\frac{V_{ij}}{V_i}\right)^{[0.2+2.6(\omega/\kappa u_*)+S_{Vi}]} \tag{14}$$

$$C_1 = \frac{Q_i}{\int_a^b q_{ij}\left(\frac{h_{ij}}{h_i}\right)^{[0.1-1.6(\omega/\kappa u_*)+1.3S_{Vi}]}\left(\frac{V_{ij}}{V_i}\right)^{[0.2+2.6(\omega/\kappa u_*)+S_{Vi}]}dy} \tag{15}$$

$$\frac{d_{cpij}}{d_{cpi}} = C_2\left(\frac{S_{ij}}{S_i}\right)^{0.6}\left(\frac{V_{ij}}{V_i}\right)^{0.1} \tag{16}$$

$$C_2 = \frac{Q_i S_i}{\int_a^b\left[q_{ij}S_{ij}\left(\frac{S_{ij}}{S_i}\right)^{0.6}\left(\frac{V_{ij}}{V_i}\right)^{0.1}\right]dy} \tag{17}$$

It should be noted that Eqs. (1)–(4) do not directly couple the liquid and solid phases, as is in fact the case between the liquid and solid phases in hyperconcentrated flows. Various researchers (Greimann et al. 1999; Ni et al. 2000) have shown that the effects of hyperconcentration should be taken into account when the depth-averaged suspended sediment concentration exceeds 100 kg/m^3. Herein, the effect of hyperconcentration is incorporated by the use of empirical parameters (such as sediment carrying capacity, etc.) in the governing equations.

Numerical Method

Preissmann four-point-difference approximations (Cunge et al. 1980) and the tridiagonal matrix algorithm are employed for solving equation systems (1) and (2). The discrete form of Eq. (3) is solved using an implicit scheme. After discretization, the riverbed deformation equation (4) becomes

$$Z_{bij}^{n+1} = Z_{bij}^n + \Delta t\frac{K_{1ij}\alpha_{*ij}}{\gamma_0}\omega_{ij}(f_{1ij}S_{ij}^{n+1} - S_{*ij}^{n+1}) \tag{18}$$

in which Δt=time step.

Boundary and Initial Conditions

Boundary conditions for the equation system given by Eqs. (1) and (2) are

$$Q_1 = Q_1(t) \text{ or } Z_1 = Z_1(t) \quad \text{(inlet condition)} \tag{19}$$

$$Z_2 = Z_2(t) \text{ or } Q_2 = f(Z_2) \quad \text{(outlet condition)} \tag{20}$$

where Q_1=inlet discharge, and Z_1=inlet water level; Q_2 and Z_2 =outlet discharge and water level, respectively.

As to the boundary conditions for the sediment transport equation, the concentration at entrance section is given. Initial conditions are determined by a series of physical parameters, such as water level, sediment concentration, and topographic features. For simplicity, these parameters are initially given estimated values. It should be noted that the approximation errors disappear quickly after the start of simulation, subject to the correct boundary conditions being implemented.

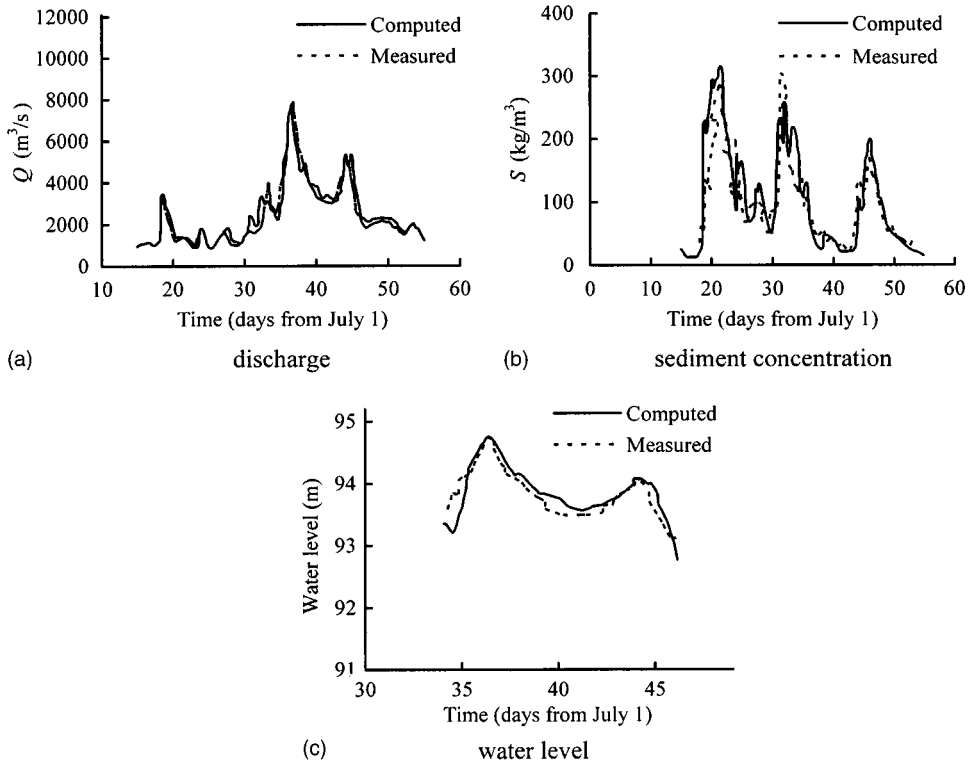

Fig. 4. Comparison of computed result and measured data at Huayuankou station, 1996

Model Validation

In 1977, 1982, and 1996, major floods occurred along the 400 km reach of the Lower Yellow River between Tiexie and Sunkou (Fig. 1). The numerical model was set up for the reach, calibrated, and validated against measured data, which is from the "Yellow River Yearbook Report" (Yellow River Conservancy Commission, 1977, 1982, and 1996). Initial and boundary conditions were determined by measured data. The topographic data are the cross sectional data along the concerned reach of the river with a distance about 10 km between two adjacent sections, obtained in the wet season before the specific flood's coming in a year. The discharge processes at Xiaolangdi upstream Tiexie, which corresponds to the specific floods, are given as inlet condition; and the rating curves at Sunkou are given as outlet condition. For the validation tests, computational grids consisting of 41 nodes in the x direction were used with spatial increment of about $\Delta x = 10{,}000$ m. The time step was $\Delta t = 900$ s.

It should be addressed that the sediment makeup in the Yellow River can be well reflected by a median diameter D_{50}, which implies a simplification with the uniform-sediment assumption in the mobile-bed equations (Chien 1988). Moreover, previous studies have revealed that suspended load is the major part and bedload is negligible in sediment-laden flows, particularly for the HCSLF (Chien 1988; Zhao 1996). Since the parameters were determined using numerous measured data obtained under different conditions, the modeling results could reflect the complex response of the HCSLF such as the extremely looped rating curve shown in Fig. 3 resulted from both bedform processes and hyperconcentration.

Good convergence is found with this grid system. Examples taken from the model validation tests are given in Figs. 4–6, where reasonable agreement between the calculated and measured results is evident. It is clear that the model properly describes hyperconcentrated floods even when the sediment concentration is higher than 100 kg/m^3 (Fig. 6). Detailed information about validation and model reliability can be seen in Zhang et al. (2001).

Radial-Basis Function–Artificial Neural Networks Model

As the rapid simulating HCSLF in the Lower Yellow River is one of the typical nonlinear processes, ANNs are introduced to speed up the simulation of the complicated HCSLF. The combination of a conventional one-dimensional mathematical model for unsteady sediment-laden flow and an ANN model for encapsulation of numerical results would be more efficient (Ni and Xue 2003). The conventional one-dimensional mathematical model provides detailed river flood routing information under typical scenarios, and the ANN model extracts numerical results from the former as training samples and validation samples to establish a station-specific model for efficient flood forecasting. The first step in the combination of the two models is to obtain detailed numerical information under typical scenarios based on the calibrated numerical model, then to design structures of the ANN model and extract training samples and validation samples from the numerical results. The third step is to train and validate the ANN model, where a neural network takes previously solved samples from the numerical model, looks for patterns in these samples, learns these patterns, and develops the ability to classify new patterns correctly. The last step is to use the ANN model to simulate if it is validated.

Among the various learning algorithms available to neural networks, the radial basis function (RBF)–ANN has the apparent advantages of learning efficiency over the more frequently used

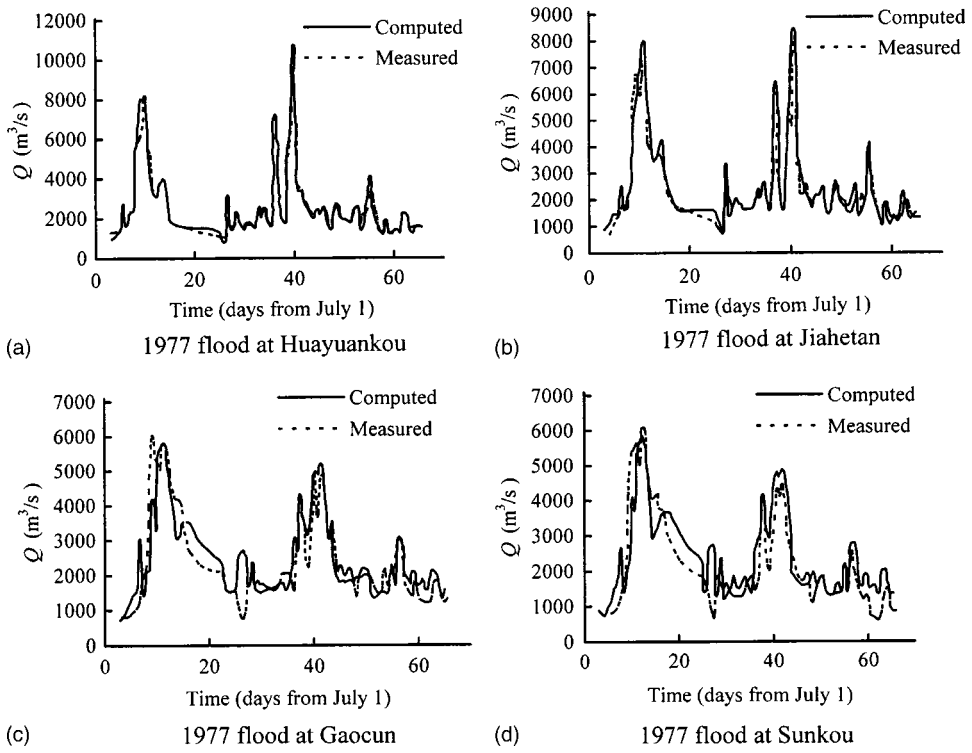

Fig. 5. Comparison of computed and measured discharge

backpropagation ANN. The RBF–ANN is often used in fields of forecasting, regression, and function interpolation (Michael and David 1998). It is particularly appropriate to the present study, due to there being sufficient samples from hydrodynamic and sediment transport models to guarantee the accuracy of the ANN model (Lohninger 1993; Dai et al. 2000). With integration of RBF–ANN and numerical modeling based on partial-differential equations in terms of the continuum concept (Li and Li 2000), the combined model has been designed to achieve rapid simulation of hyperconcentrated floods.

The RBF–ANN for HCSLF in the Yellow River includes models for discharge, water level, and sediment concentration. It should be noted that there are two categories of the model that are considered in the present paper. The "station-specific" ANN model establishes a relationship between a single desired station and the entrance station, whereas the "one-dimensional" ANN model establishes a relationship between multiple stations and the entrance station. The system is truly time varying and has strong time-delayed phenomena. In order to simulate the time-delayed phenomena correctly, in the ANN model for discharge (e.g., at Huayuankou), the serial discharge Q is sampled as a sequence of five temporal values before time t as the input nodes of the ANN model. Initially, there are 12 hidden layers, which are naturally adjusted to the proper number of nodes during the ANN training process. The output layer calculates one new discharge at time t. So the arrangement of input, hidden, and output nodes are 5, 12, and 1, respectively. Although the station-specific model is highly efficient for discharge evaluation at a particular station under consideration, it is not suitable for simulation of the whole process at all stations, which should be accomplished by a hydrodynamic model. Nevertheless, a one-dimensional ANN model could be established through extending the number of nodes in the input layer based on a station-specific model (five discharge inputs) with an additional five inputs of distance ordinate x, sediment carrying capacity $S*$, saturation recovery coefficient $\alpha*$, riverbed roughness n, and cross sectional width b. All the foregoing input

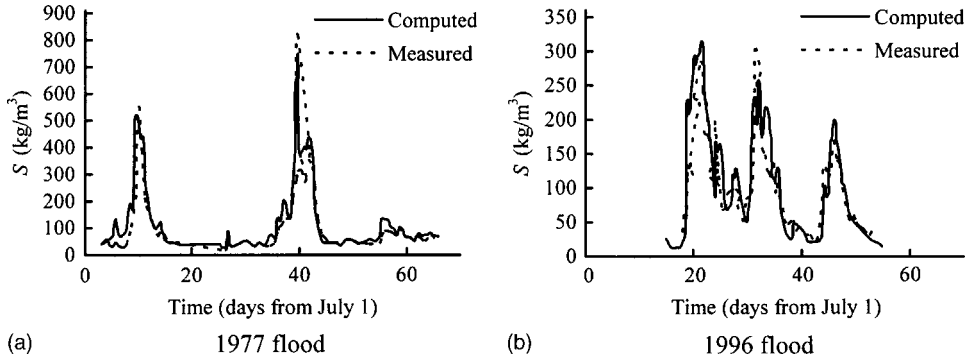

Fig. 6. Comparison of computed and measured sediment concentration at Huayuankou

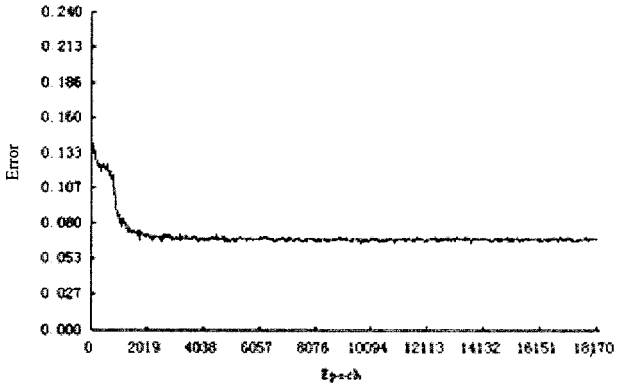

Fig. 7. Error decay process in training of discharge artificial neural networks at Huayuankou

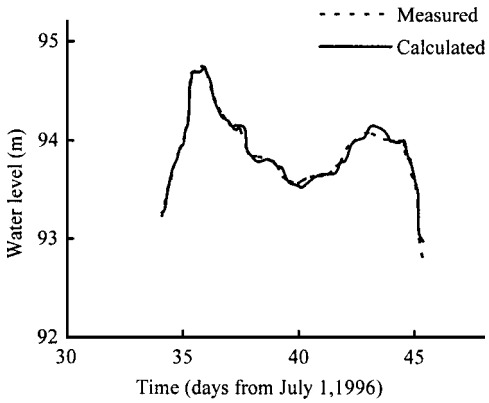

Fig. 9. Comparison of artificial neural networks computed and measured water levels at Huayuankou

parameters are time dependent and are selected to denote the difference between stations. The numbers of nodes for the one-dimensional model then become 10, 12, 1, for the input layer, hidden layer, and output layer, respectively.

Encapsulation of Station-Specific Knowledge

For any given station, evaluated and validated values of water level and discharge at certain time steps can be extracted from the one-dimensional hydrodynamic model. To guarantee wide adaptability of the ANN model, typical Lower Yellow River boundary conditions are provided from the 1977, 1982, and 1996 flood data. The numerical model results under these representative flood scenarios provide an adequate sample of data sets for the neural networks. Thus a rapid response is established between discharge, water level and sediment concentration. For the station-specific ANN model, 250 training samples and 50 validation samples are selected from numerical results at the Huayuankou, Jiahetan, Gaocun, and Shunkou stations. For the one-dimensional ANN model, 1,000 training samples and 200 validation samples are extracted from numerical modeling results.

Evaluation and Verification of Artificial Neural Network Model

The system root mean square error decreases within the training process. Fig. 7 illustrates a typical error decay process (obtained using the Huayuankou station-specific ANN model). After, 5,000 iterations, the training process of the ANN models become stable, and the root mean square error only changes 0.002 from iteration 5,000 to 18,000. It is obvious that 5,000 training iterations is enough to construct a stable ANN model, but further training iterations will not lead to an overtraining state.

Fig. 8 shows the close agreement achieved between the predicted discharges obtained using the ANN model and the input (validation) measurements at Huayuankou. An indication of the performance of the training set is that the root mean square error of the ANN model is about than 7.2%. The overall precision is 92.8% (1 rms error). Figs. 9 and 10 provide validation results for water levels and sediment concentrations at Huayuankou. The validation set for the ANNs (Fig. 9) is of the same length as that for the numerical model validation (Fig. 4) because the same data set was used in both cases. It is evident that the ANN models reproduce properly the output of the numerical model, with which they were trained.

Improvement of Computational Speed

All computations have been performed on a PC with CPU 866 MHz and RAM of 128 M under the *Windows 2000* Professional operating system. The CPU time is less than 11 s for station-specific models and less than 27 s for one-dimensional models in order to calculate discharge, water level, and sediment concentration at Huayuankou, Jiahetan, Gaocun, and Sunkou with the ANN. The CPU time for the RBF–ANN model is approxi-

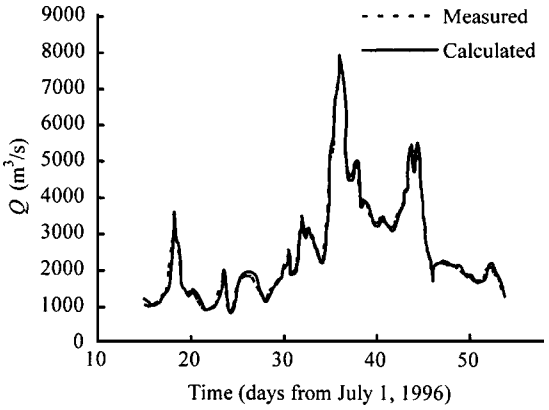

Fig. 8. Comparison of artificial neural networks computed and measured discharge at Huayuankou

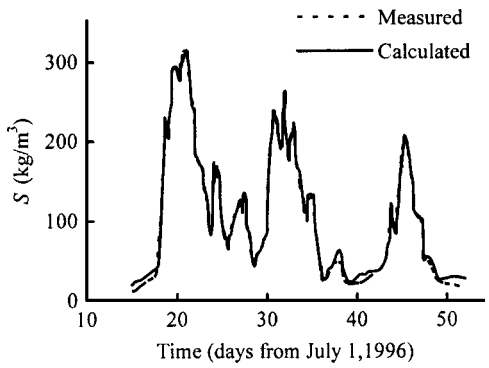

Fig. 10. Comparison of artificial neural networks computed and measured sediment concentration at Huayuankou

mately 50 times faster than the corresponding one-dimensional hydrodynamic model. It is therefore found that the combination of the conventional hydrodynamic numerical model and ANN leads to considerable efficiency gains.

Conclusions

Hyperconcentrated sediment-laden flows have very different characteristics to low-concentrated sediment laden flows, and are inherently more difficult to predict, prevent, or control. Due to differences in the solid–liquid flow physics, conventional mathematical models developed for low-concentrated sediment-laden floods are not applicable to hyperconcentrated floods. Herein, a model that integrates a conventional one-dimensional mathematical model for unsteady sediment-laden flow and an ANN has been developed. In the present uncoupled model, the effect of hyperconcentration is necessarily incorporated through the calibration of the numerical model to the field data through empirical parameters (such as sediment carrying capacity, etc.). In future work, it would be better to develop a fully coupled numerical model and use it to train the ANN model.

The model provides a rapid-response forecast tool applicable to varying flow and sediment conditions. Three typical floods occurring in 1977, 1982, and 1996 in the Lower Yellow River have been used to evaluate and validate the model. It has been demonstrated that the numerical results closely fit the measured data. The computational speed has been significantly improved, confirming the practical applicability of the hybrid model to rapid estimation of hydraulic and sediment parameters (such as discharge, water level, and sediment concentration). The present model is appropriate to both hyperconcentrated and low-concentrated sediment-laden floods. Station-specific ANN models trained with data from a specific time period may become increasingly inaccurate at predicting future scenarios if the river reach changes its bed morphology considerably due to erosion and deposition. Future work is required to develop ANN models that are retrained as and when new data are available, and are biased towards the most recent information.

Acknowledgments

Financial support for this research has been provided by the National Natural Science Foundation and Ministry of Water Resources of China under Grant No. 59890200. Thanks are to L.J. Zhao and Dr. Y.D. Huang for their kind help in the preparation of this paper.

Notation

The following symbols are used in this paper:

A = cross-sectional area (m^2);
B = flow width at free surface (m);
b = empirical coefficient;
C = Chézy resistance coefficient;
C_1, C_2 = functions as defined in Eq. (15) and (17), respectively;
c_n = $c_n = 0.375\ \kappa$, vortex coefficient;
D_{50} = median diameter of bed material (m);
d_{cp} = average diameter of suspended material (m);
d_{50} = median diameter of suspended material (m);
F = $\mathrm{F} = V/(gh)^{1/2}$, Froude number;
f = function as defined in Eq. (7);
f_1 = subsaturation coefficient as defined in Eq. (9);
g = gravitational acceleration (m/s^2);
h = water depth (m);
K = discharge modulus;
K_1 = comprehensive coefficient as defined in Eq. (8);
N_0 = integral function as defined in Eq. (6);
n = Manning's roughness coefficient;
Q = flow discharge (m^3/s);
q = flow discharge per unit width (m^2/s);
q_L = lateral water inflow per unit length (m^2/s);
S = sediment concentration (kg/m^3);
S^* = sediment carrying capacity (kg/m^3);
S_L = lateral sediment inflow per unit length;
S_V = particle volume fraction;
t = time (s);
u^* = friction velocity (m/s);
V = flow velocity (m/s);
x = spatial variable (m);
y = coordinate in transversal direction (m);
Z = water level (m);
Z_b = bed elevation (m);
α^* = saturation recovery coefficient;
α_1, α_2 = momentum correction factors;
γ = specific weight of water;
γ_m = specific weight of muddy water; $\gamma_m = \gamma + S(\gamma_s - \gamma)/\gamma$;
γ_S = specific weight of sediment;
γ_0 = dry weight of sediment;
Δt = time step (s);
δ^* = friction thickness (m);
η = relative depth;
κ = Kármán universal constant;
ω = settling velocity of sediment particles (m/s); and
ω_0 = settling velocity of sediment particles in clear water (m/s).

References

Chen, X.T., Chen, M.F., and Song, X.J. (2000). "Influence of sediment concentration to deposition of chemical in the Lower Yellow River." *J. Yellow River*, 22(11), 13–14 (in Chinese).

Chien, N. (1988). *Hyper-concentrated flow*, Tsinghua Univ. Press, Beijing.

Cunge, J.A., Holley, F.M., Jr., and Verwey, A. (1980). *Practical aspects of computational river hydraulics*, Pitman, London.

Dai, Y., Lu, Y., Zhang, A.Q., and Han, S.K. (2000). "Prediction of bioactivity of organic compounds by a neural network based on radial basis functions." *Environmental Sci.*, 21(4), 11–15 (in Chinese).

Greimann, B.P., Muste, M., and Holly, F.M. (1999). "Two-phase forulation of suspended sediment transport." *J. Hydraul. Res.*, 37(4), 479–500.

Hsu, K.L., Gupta, H.V., and Sorooshian, S. (1995). "Artificial neural network modeling of the rainfall-runoff process." *Water Resour. Res.*, 31, 2517–2530.

Li, R., and Li, Y.T. (1999). "Applied researches of neural network in flood prediction." *Int. J. Sediment Research*, 14(2), 237–242.

Li, R., and Li, Y.T. (2000). "Application of neural networks to sediment-laden flow." *J. Hydraul. Eng.*, 6, 115–121 (in Chinese).

Lin, B. L., and Falconer, R. A. (1996). "Numerical modeling of three dimensional suspended sediment for estuarine and coastal waters." *J. Hydraul. Res.*, 34(4), 435–456.

Lin, P. N., Huan, J. Q., and Li, X. Q. (1983). "Unsteady transport of suspended load at small concentrations." *J. Hydraul. Eng.*, 109(1),

86–98.
Lohninger, H. (1993). "Evaluation of neural networks based on radial basis functions and their application to the prediction of boiling points form structural parameters." *J. Chem. Inf. Comput. Sci.*, 33(5), 736–744.
Michael, E.T., and David, L. (1998). "A novel algorithm for topographic projections by radial basis functions." *Neurocomputing*, 19, 211–222.
Minns, A.W., and Hall, M. J. (1996). "Artificial neural networks as rainfall-runoff models." *J. Hydrology Sci.*, 41, 399–417.
Ni, J.R., Wang, G.Q., and Borthwick, A. G. L. (2000). "Kinetic theory for particles in dilute and dense solid-liquid flows." *J. Hydraul. Eng.*, 126(12), 893–903.
Ni, J. R., and Xue, A. (2003). "Application of artificial neural network to the rapid feedback of potential ecological risk in flood diversion zone." *Eng. Applic. Artif. Intell.*, 16(2), 105–119.
Wei, Z.L. (1990). "Two-dimensional mathematical model for sediment-laden flow in the Lower Yellow River." *Research Rep. Prepared for Wuhan Univ.*, Wuhan, China (in Chinese).
Yellow River Conservancy Commission (1977, 1982, and 1996). *Yellow River Yearbook Rep.*, Ministry of Water Resources, Beijing (in Chinese).
Yonas, B.D., and Michael, B.A. (1999). "Application of artificial neural networks to the simulation of a two-dimensional flow." *J. Hydraul. Res.*, 37(4), 435–447.
Zhang, H.W., Huang, Y.D., and Zhao, L.J. (2001). "A mathematical model for unsteady sediment transport in the lower yellow river." *Int. J. Sediment Res.*, 16(2), 150–158.
Zhang, H.W., and Zhang, Q. (1992). "The formula for sediment carrying capacity of flow in the Yellow River." *J. Yellow River*, 11, 7–9 (in Chinese).
Zhao, W.L. (1996). *Sediments in the Yellow River*, The Yellow River Conservancy Commission, Zhengzhou (in Chinese).